JNM The Journal of NUCLEAR MEDICINE

Novel ^{18}F-Labeled Arylquinoline Derivatives for Noninvasive Imaging of Tau Pathology in Alzheimer Disease

Nobuyuki Okamura, Shozo Furumoto, Ryuichi Harada, Tetsuro Tago, Takeo Yoshikawa, Michelle Fodero-Tavoletti, Rachel S. Mulligan, Victor L. Villemagne, Hiroyasu Akatsu, Takayuki Yamamoto, Hiroyuki Arai, Ren Iwata, Kazuhiko Yanai and Yukitsuka Kudo

J Nucl Med. 2013;54:1420-1427.
Published online: July 15, 2013.
Doi: 10.2967/jnumed.112.117341

The Journal of Nuclear Medicine is published monthly.
SNMMI | Society of Nuclear Medicine and Molecular Imaging
1850 Samuel Morse Drive, Reston, VA 20190.
(Print ISSN: 0161-5505, Online ISSN: 2159-662X)

SNMMI SOCIETY OF NUCLEAR MEDICINE AND MOLECULAR IMAGING

Novel ^{18}F-Labeled Arylquinoline Derivatives for Noninvasive Imaging of Tau Pathology in Alzheimer Disease

Nobuyuki Okamura[1], Shozo Furumoto[1,2], Ryuichi Harada[1], Tetsuro Tago[2], Takeo Yoshikawa[1], Michelle Fodero-Tavoletti[3], Rachel S. Mulligan[4], Victor L. Villemagne[4], Hiroyasu Akatsu[5], Takayuki Yamamoto[5], Hiroyuki Arai[6], Ren Iwata[2], Kazuhiko Yanai[1], and Yukitsuka Kudo[7]

[1]Department of Pharmacology, Tohoku University School of Medicine, Sendai, Japan; [2]Division of Radiopharmaceutical Chemistry, Cyclotron and Radioisotope Center, Tohoku University, Sendai, Japan; [3]Department of Pathology, University of Melbourne, Victoria, Australia; [4]Department of Nuclear Medicine and Centre for PET, Austin Health, Melbourne, Victoria, Australia; [5]Choju Medical Institute, Fukushimura Hospital, Toyohashi, Japan; [6]Department of Geriatrics and Gerontology, Institute of Development, Aging and Cancer, Tohoku University, Sendai, Japan; and [7]Clinical Research, Innovation and Education Center, Tohoku University Hospital, Sendai, Japan

Neurofibrillary tangles in Alzheimer disease (AD) brains are composed of the microtubule-associated protein tau. Noninvasive monitoring of tau protein aggregates in the living brain will provide useful information regarding tau pathophysiology in AD. However, no PET probes are currently available for selective detection of tau pathology in AD. We have previously reported ^{18}F-labeled THK-523 (^{18}F-6-(2-fluoroethoxy)-2-(4-aminophenyl)quinoline) as a tau imaging radiotracer candidate for PET. After compound optimization, we developed novel ^{18}F-labeled arylquinoline derivatives, ^{18}F-THK-5105 and ^{18}F-THK-5117, for use as tau imaging PET tracers. **Methods:** ^{18}F-labeled compounds were prepared from the corresponding tosylated precursors. The binding affinity of compounds to synthetic tau aggregates and tau-rich AD brain homogenates was determined by saturation and competition binding assays. The binding selectivity of compounds to tau pathology was evaluated by autoradiography of AD brain sections. The pharmacokinetics of compounds were assessed in biodistribution studies in normal mice. A 14-d toxicity study with intravenous administration of compounds was performed using rats and mice. **Results:** In vitro binding assays demonstrated higher binding affinity of THK-5105 and THK-5117 than THK-523 to tau protein aggregates and tau-rich AD brain homogenates. Autoradiographic analyses of AD brain sections showed that these radiotracers preferentially bound to neurofibrillary tangles and neuropil threads, which colocalized with Gallyas-positive and immunoreactive tau protein deposits. The distribution of this radiotracer binding in AD brain sections was completely different from that of ^{11}C-Pittsburgh compound B, showing preferential binding to amyloid plaques. Furthermore, these derivatives demonstrated abundant initial brain uptake and faster clearance in normal mice than ^{18}F-THK-523 and other reported ^{18}F-labeled radiotracers. THK-5105 and THK-5117 showed no toxic effects related to the administration of these compounds in mice and rats and no significant binding for various neuroreceptors, ion channels, and transporters at 1-μM concentrations. **Conclusion:** ^{18}F-labeled THK-5105 and THK-5117 are promising candidates as PET tau imaging radiotracers.

Key Words: Alzheimer disease; tau; neurofibrillary tangles; positron emission tomography; molecular imaging

J Nucl Med 2013; 54:1420–1427
DOI: 10.2967/jnumed.112.117341

Alzheimer disease (AD) is the most common cause of dementia in the elderly. At present, approximately 18 million people worldwide have AD, and this number is estimated to double by 2025 (*1*). The major pathologic hallmarks of AD are senile plaques (SPs) and neurofibrillary tangles (NFTs). SPs are composed of amyloid-β protein (Aβ), a 39–43 amino acid protein product derived from the proteolytic cleavage of the amyloid precursor protein. Abnormalities in the production or clearance of Aβ are considered to be the initiating events in AD pathogenesis (*2*). Excessive Aβ concentrations lead to its aggregation and formation of SPs, followed by NFT formations, synaptic dysfunction, and neuronal death. NFTs are composed of hyperphosphorylated tau, a microtubule-associated protein that stabilizes microtubule assembly in axons (*3*). Tau accumulation is also recognized as neuropil threads and dystrophic neurites in the AD brain (*4*). Phosphorylation of tau decreases its ability to bind to microtubules, which are destabilized, leading to neuronal death. NFT lesions follow a stereotypical pattern, initially appearing in the transentorhinal cortex, followed by the entorhinal cortex and the hippocampus, and subsequently the neocortex (*5*). In AD patients, the severity of tau pathology is closely related to neuronal loss (*6,7*) and cognitive impairment (*8,9*). The deposition of NFTs is thought to begin before extensive neuronal loss and cognitive decline occur. Thus, noninvasive detection of tau pathology would be useful to predict future cognitive decline in the preclinical stages of AD and to track disease progression before extensive neuronal loss occurs.

Several researchers have focused on developing radiotracers for imaging tau pathology in the human brain (*10–17*). Tau imaging radiotracers need to cross the blood–brain barrier and to have a high binding affinity to NFTs with minimal nonspecific binding (*18*). 2-(1-(6-[(2-^{18}F-fluoroethyl)(methyl)amino]-2-naphthyl)ethylidene)malononitrile (^{18}F-FDDNP) is claimed as the only PET tracer that allows measurement of the amount of tau protein

Received Nov. 19, 2012; revision accepted Feb. 19, 2013.
For correspondence or reprints contact: Nobuyuki Okamura, 2-1, Seiryo-machi, Aoba-ku, Sendai 980-8575 Japan.
E-mail: nookamura@med.tohoku.ac.jp
Published online Jul. 15, 2013.

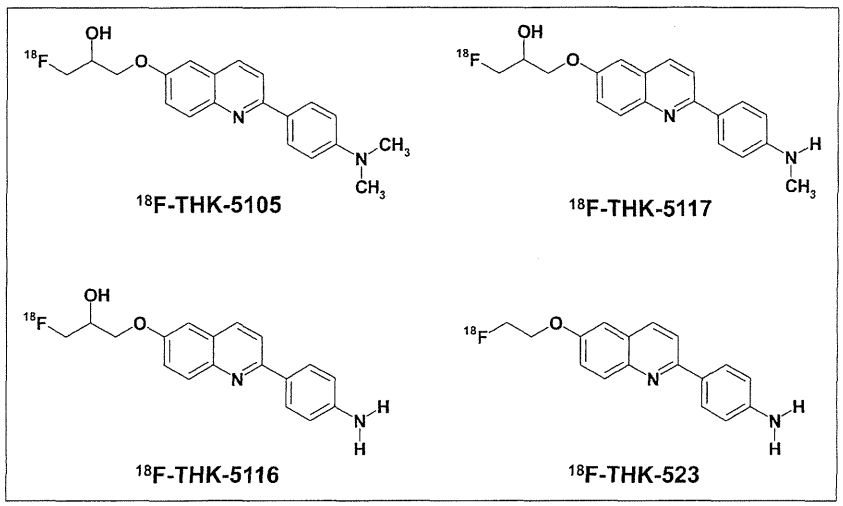

FIGURE 1. Chemical structures of ^{18}F-THK-5105, ^{18}F-THK-5116, ^{18}F-THK-5117, and ^{18}F-THK-523.

deposits in the human brain (*19*). However, ^{18}F-FDDNP was found to have lower binding affinity for protein fibrils than ^{11}C-Pittsburgh compound B (^{11}C-PiB) (*20,21*). In addition, this tracer has been claimed to bind to both SPs and NFTs equally (*22*). In the neocortex of the AD brain, SPs and NFTs colocalize with each other, where Aβ concentrations are 5–20 times higher than that of tau (*23,24*). In such cases, the signal from the SPs would be so overwhelming that it would obscure the signal from the NFTs. Therefore, the development of selective tau imaging tracers is necessary for accurate and quantitative evaluation of tau pathology in AD.

In the past few years, we also have screened more than 2,000 compounds to develop novel radiotracers with high affinity and selectivity for tau aggregates. Consequently, we identified a series of novel quinoline and benzimidazole derivatives that bind NFTs and, to a lesser extent, Aβ plaques (*10*). Serial analyses of these compounds led to the design and synthesis of the novel tau imaging agent ^{18}F-6-(2-fluoroethoxy)-2-(4-aminophenyl)quinoline (^{18}F-THK-523) (*15,17*). Preclinical analyses of ^{18}F-THK-523 indicated that this tracer selectively labels tau pathology in the AD brain. However, the preclinical data suggest that the pharmacokinetics and binding characteristics of ^{18}F-THK-523 might not reach the necessary optimal levels required for PET tracers. Through our optimization process, we developed novel ^{18}F-labeled 2-arylquinoline derivatives that are promising candidates for in vivo tau imaging probes. In this study, we performed the preclinical evaluation of the binding and pharmacokinetic properties of these compounds.

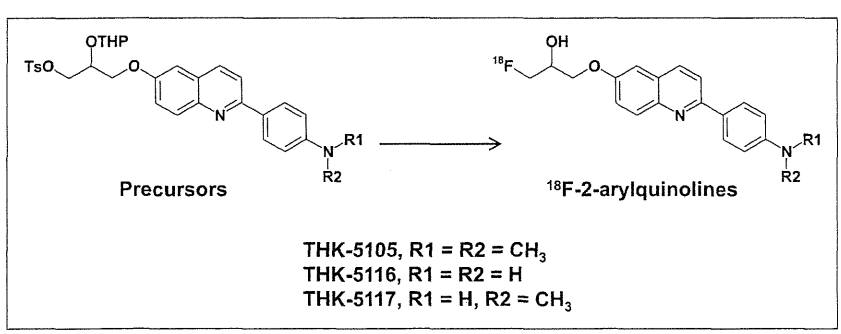

FIGURE 2. Radiosynthesis scheme of ^{18}F-2-arylquinolines.

MATERIALS AND METHODS

Synthesis and Radiosynthesis of 2-Arylquinoline Derivatives

The chemical structures of 6-[(3-^{18}F-fluoro-2-hydroxy)propoxy]-2-(4-dimethylaminophenyl)quinoline (^{18}F-THK-5105), 6-[(3-^{18}F-fluoro-2-hydroxy)propoxy]-2-(4-methylaminophenyl)quinoline (^{18}F-THK-5117), 6-[(3-^{18}F-fluoro-2-hydroxy)propoxy]-2-(4-aminophenyl)quinoline (^{18}F-THK-5116), and ^{18}F-THK-523 are shown in Figure 1. ^{18}F-THK-5105, ^{18}F-THK-5116, and ^{18}F-THK-5117 were prepared from the corresponding tosylate precursors according to the scheme as indicated in the Figure 2. Details on their syntheses will be described elsewhere (S. Furumoto et al., unpublished data, 2013). Briefly, the aqueous $^{18}F^-$ contained in the K_2CO_3 solution (1.59–3.69 GBq) and Kryptofix222 (15 mg) were placed in a brown vial. Water was removed by azeotropic evaporation with acetonitrile. After being dried, the activated ^{18}F-KF/Kryptofix222 was reacted with the precursor (3 mg) in dimethylsulfoxide (0.7 mL) at 110°C for 10 min. Then, 2 M HCl was added to the solution, followed by an additional 3-min reaction for deprotection of the hydroxyl group. After neutralization with 4 M AcOK, the product was purified by semipreparative high-performance liquid chromatography (HPLC) (column: Inertsil ODS-4 [GL Sciences, Inc.]; mobile phase: 20 mM NaH_2PO_4/acetonitrile [55/45 for THK-5105 and THK-5117, 65/35 for THK-5116]; flow rate: 5.0 mL/min). The radiolabeled product was dissolved in ethanol, dimethylsulfoxide, or saline with polysobate-80 (<0.1%) for biologic evaluation.

^{18}F-THK-523 and ^{18}F-FDDNP were also prepared in a manner similar to the one described above using the corresponding tosylate precursors reported previously (*15,25,26*). ^{11}C-PiB was radiolabeled using its precursor (2-(4-aminophenyl)-6-methoxymethoxybenzothiazole) and ^{11}C-methyl triflate, as previously described (*27*).

Determination of Log P Values

Log P values were determined by the HPLC method according to the guideline of the Organisation for Economic Co-operation and Development (OECD Guideline for Testing of Chemicals: Partition Coefficient (n-octanol/water), High Performance Liquid Chromatography [HPLC] Method), with slight modification. Briefly, 12 reference compounds whose log P values ranged between 0.5 and 4.0 were analyzed by HPLC under the following conditions: HPLC, a JASCO LC-2000 Plus series (JASCO); column, Inertsil ODS-4 (4.6 × 150 mm, 5 μm; GL Sciences, Inc.); mobile phase, 20 mM NaH_2PO_4 (pH 7.4)/acetonitrile (55/45); flow rate, 1.5 mL/min; ultraviolet absorbance, 245 nm; and column temperature, 40°C. Then, a calibration curve of log (tR − t0) (tR, retention time; t0, dead time) versus log P of each reference compound was created (R^2 = 0.9469). Test compounds listed in Table 1 were also analyzed by the same HPLC method to measure log (tR − t0) values that were used for determination of log P values from the calibration curve.

In Vitro Binding Assays

Synthetic human Aβ1–42 was purchased from Peptide Institute Inc. Recombinant K18ΔK280-tau protein was obtained from Life Technologies Japan Ltd. Fibrils of

TABLE 1
Log P and Brain Uptake After Intravenous Administration of ^{18}F-Labeled Compounds in Mice

Compound	Log P	Brain uptake (%ID/g)			Brain uptake ratio (2 min/60 min)
		2 min after injection	30 min after injection	60 min after injection	
^{18}F-THK-523	2.40	2.72	1.47	1.46	1.86
^{18}F-THK-5105	3.03	9.20	3.61	1.00	9.20
^{18}F-THK-5116	1.57	3.36	0.75	0.57	5.89
^{18}F-THK-5117	2.32	6.06	0.59	0.26	23.1
^{18}F-FDDNP	3.71	6.23	2.02	2.14	2.91

Aβ1–42 and K18ΔK280-tau were prepared as described previously (*15*). Briefly, synthetic Aβ1–42 (200 μM) and K18Δ280K-tau (20 μM) solutions in phosphate-buffered saline (PBS) were incubated at 37° C with agitation for 3–4 d. We additionally prepared AD brain homogenates for binding assay, because the structural conformation of synthetic protein fibrils does not fully correlate with the structure of native protein deposits in the human brain. Human brain tissue was isolated from a mesial temporal frozen sample of an AD patient and homogenized in PBS. Brain tissue homogenate aliquots were taken and frozen at −80°C until used. Insoluble Aβ and tau levels were determined using a human β-amyloid enzyme-linked immunosorbent assay (ELISA) kit (Wako) and a human tau ELISA kit (Life Technologies Japan Ltd.), respectively. Next, brain homogenates and the solutions of synthetic Aβ1–42 or K18Δ280K-tau fibrils were incubated with increasing concentrations of ^{18}F-THK-5105 (0.1–250 nM). To account for nonspecific binding of ^{18}F-THK-5105, the reactions were performed in triplicate in the presence of 2 μM unlabeled THK-5105. The binding reactions were incubated for 1 h at room temperature in assay buffer (Dulbecco PBS; 0.1% bovine serum albumin). Bound radioactive compounds were separated from free radioactive compounds by filtration under reduced pressure (MultiScreen HTS Vacuum Manifold; Millipore). Filters were washed three times with assay buffer, and the radioactivity contained within the filters was counted in a γ-counter (AccuFLEX γ7000, Aloka, Tokyo, Japan). Binding data were analyzed using curve-fitting software that calculates the K_d and B_{max} (K_d is dissociation constant and B_{max} is maximum number of binding sites, respectively) using nonlinear regression (GraphPad Prism; GraphPad Software).

For inhibition studies, the assay buffer containing each compound (0.1–1,000 nM), ^{18}F-THK-5105 (1.76 nM, ~37 kBq), K18Δ280K-tau (200 nM), and 0.1% bovine serum albumin was incubated at room temperature for 1 h. Nonspecific binding was determined in the presence of 10 μM THK-5105. The mixture was filtered through Multiscreen HTS 96-well filtration plates, followed by washing three times with PBS (0.1% bovine serum albumin), and the filters containing bound ^{18}F ligand were counted in a γ-counter. The percentage of bound radioligand at each concentration was measured in triplicate and then plotted against the inhibitor concentration. Half-maximal inhibitory concentration values were determined from the displacement curves using the GraphPad Prism software. Inhibition constant (K_i) values were calculated from the half-maximal inhibitory concentration values using the Cheng–Prusoff equation (*28*).

TABLE 2
K_d and B_{max} Values of ^{18}F-THK-5105 for Synthetic Tau and $Aβ_{1-42}$ Fibrils

Protein	K_{d1}	B_{max1}	K_{d2}	B_{max2}
Tau	1.45	6.89	7.40	20.05
$Aβ_{1-42}$	35.9	61.6		

K_d are in nM and Bmax are in pmol ^{18}F-THK-5105/nmol fibrils.

Tissue Staining

Experiments were performed under the regulations of the ethics committee of Tohoku University School of Medicine. Paraffin-embedded hippocampal brain sections from an autopsy-confirmed AD case (78-y-old woman) were used for tissue staining with THK-5105. Brain sections were obtained from Fukushimura Hospital. After deparaffinization, autofluorescence quenching was performed as previously described (*29*). Quenched tissue sections were immersed for 10 min in a 100-μM THK-5105 solution containing 50% ethanol. Sections were then dipped briefly into water, rinsed in PBS, coverslipped with FluorSave Reagent (Calbiochem), and examined using an Eclipse microscope (Nikon) equipped with a blue-violet filter (excitation, 400–440 nm; dichroic mirror, 455 nm; barrier filter, 470 nm). Sections stained with THK-5105 were subsequently immunostained with the AT8 anti-tau antibody (diluted 1:20; Innogenetics). After incubation at 4°C in the primary antibody for 16 h, sections were processed by the avidin-biotin method using a Pathostain ABC-POD(M) Kit (Wako) and diaminobenzidine as a chromogen. Sections were additionally stained using a modified Gallyas–Braak method (pretreatment with 0.3% potassium permanganate for 10 min, followed by 0.1% oxalic acid for 3 min) (*30*).

Autoradiography of Human Brain Sections

For the autoradiographic study, 8-μm-thick paraffin-embedded brain sections from a healthy control (62-y-old man) and 2 AD patients (69-y-old man and 92-y-old woman) were used. After deparaffinization, sections were incubated for 10 min at room temperature with radiolabeled compounds (0.5 MBq/mL) and washed briefly with water and 50% ethanol. After being dried, the labeled sections were exposed overnight to a BAS-III imaging plate (Fuji Film). The autoradiographic images were obtained using a BAS-5000 phosphoimaging instrument (Fuji Film). The neighboring sections were stained

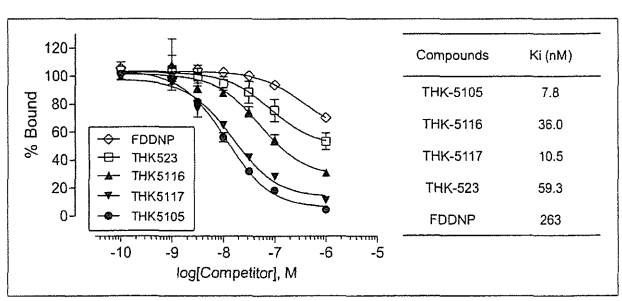

FIGURE 3. Competitive inhibition of ^{18}F-THK-5105 binding by 2-arylquinolines and FDDNP to tau protein fibrils. K_i values for inhibition of ^{18}F-THK-5105 binding to tau are shown.

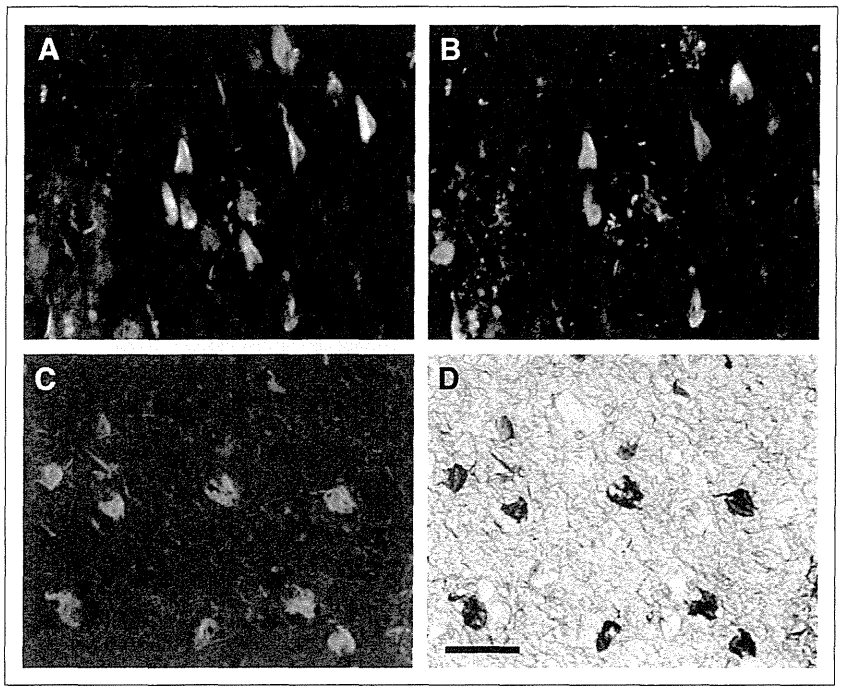

FIGURE 4. *Neuropathologic staining of brain sections from AD patients. Neurofibrillary tangles and neuropil threads were clearly stained with THK-5105 (A and C). These stainings were consistent with tau immunostaining (B) and Gallyas–Braak staining (D) in same sections. Bar = 50 μm.*

using a modified Gallyas–Braak method or immunostained using the AT8 anti-tau monoclonal antibody (diluted 1:20; Innogenetics), the 4G8 Aβ antibody (diluted 1:100; Signet), or the 6F/3D Aβ antibody (diluted 1:50; Dako). For correlational analysis of the autoradiographic and immunohistochemical images, 36 circular regions of interest (the area of each region of interest was ~7 mm^2) were placed on the gray matter of the hippocampus, parahippocampal gyrus, fusiform gyrus, temporal gyri (superior, middle, and inferior), insula, pre- and postcentral gyri, superior frontal gyrus, paracentral lobule, and cingulate gyrus. The percentage area of positive signals in each region of interest was calculated using ImageJ software (National Institutes of Health). A correlational analysis between percentage areas of tracer binding and positive immunostaining was performed using Pearson simple correlation.

Biodistribution in Mice

The experimental protocol of animal study was approved by the Ethics Committee of Tohoku University School of Medicine. ^{18}F-labeled tracers (1.1–6.3 MBq) were injected into the tail vein of male ICR mice (n = 20; mean weight, 28–32 g). Mice were then sacrificed by decapitation at 2, 10, 30, 60, and 120 min after injection. The brain, blood, liver, kidney, and femur were removed and weighed, and radioactivity was counted with an automatic γ-counter. The percentage injected dose per gram of tissue (%ID/g) was calculated by comparing tissue counts to tissue weight. Each %ID/g value is expressed as a mean ± SD of 4 separate experiments.

Animal Toxicity Studies

A 14-d toxicity study with intravenous administration of a single dose of THK-5105 and THK-5117 was performed using Sprague–Dawley rats and ICR mice. Briefly, the study included 3 groups of male and female rats and mice that were administered 0 (group 1), 0.1 (group 2), and 1 (group 3) mg/kg of test article (10% dimethylsulfoxide/90% distilled water) per rat or mouse by intravenous injection on study day 1. The study included clinical observations plus body weight measurements for a 14-d observation period. Hematology and pathologic examinations were conducted on study days 2 and 15. Detailed necropsies with external examinations were also performed.

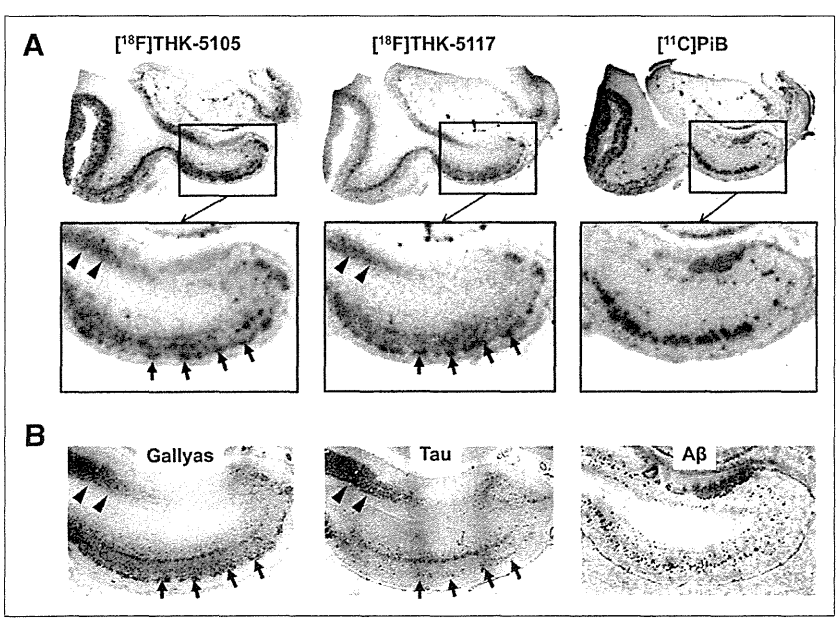

FIGURE 5. *(A) Autoradiographic images of ^{18}F-THK-5105, ^{18}F-THK-5117, and ^{11}C-PiB binding in mesial temporal section from AD patient. (B) Gallyas–Braak silver staining (left) and immunostaining with anti-tau (center) and anti-Aβ (right) antibodies in adjacent brain sections. Arrowheads = CA1 area of hippocampus; longer arrows = entorhinal cortex.*

Receptor Binding Assays

Receptor binding screens were conducted by Sekisui Medical Inc. Binding inhibition effects of 1 μM THK-5105 and THK-5117 were evaluated in competitive radioligand assays against 60 common neurotransmitter receptors, ion channels, and transporters. Percentage inhibition ratios were calculated by the following equation: inhibition ratio (%) = $[1 - (B - N)/(B_0 - N)] \times 100$, where N is the nonspecific bound radioactivity, and B and B_0 are the bound radioactivity in the presence and absence of tested compounds, respectively. Data are expressed as the mean values of duplicate samples.

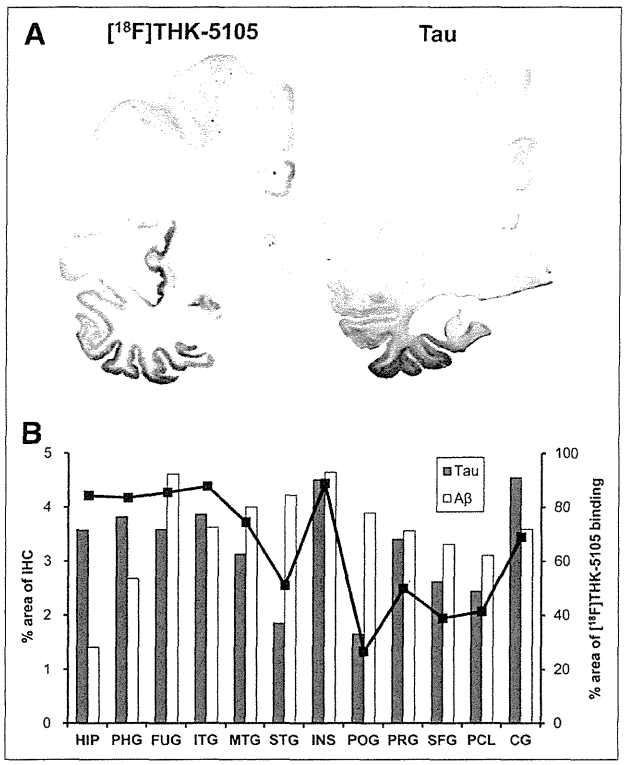

FIGURE 6. (A) Autoradiography of hemibrain sections from AD patient with ^{18}F-THK-5105 and tau immunostaining in neighboring section. (B) Region-of-interest analysis indicated that percentage areas of ^{18}F-THK-5105 binding (line plots) were significantly correlated with percentage areas of tau immunostaining (gray bars) but not with that of Aβ immunostaining (white bars). CG = cingulate gyrus; HIP = hippocampus; FUG = fusiform gyrus; IHC = immunohistochemistry; INS = insula; ITG = inferior temporal gyrus; MTG = middle temporal gyrus; PCL = paracentral lobule; PHG = parahippocampal gyrus; POG = postcentral gyrus; PRG = precentral gyrus; SFG = superior frontal gyrus; STG = superior temporal gyrus.

RESULTS

Radiosynthesis

All radiolabeled compounds were obtained in greater than 97% radiochemical purities after HPLC purification. The decay-corrected average radiochemical yields of ^{18}F-THK-523, ^{18}F-THK-5105, ^{18}F-THK-5116, ^{18}F-THK-5117, and ^{18}F-FDDNP were 58%, 48%, 41%, 48%, and 22%, respectively. The specific activities of ^{18}F-labeded compounds ranged from 37 to 110 GBq/μmol, corrected at the end of synthesis. The mean specific activity of ^{11}C-PiB was 35 GBq/μmol.

In Vitro Binding Assays

The binding properties of phenylquinoline derivatives to tau fibrils was investigated and compared with Aβ1–42 fibrils. Although only a single class of ^{18}F-THK-5105 binding sites was identified on Aβ1–42 fibrils, 2 classes of ^{18}F-THK-5105 binding sites were identified on K18Δ280-tau fibrils. As shown in Table 2, the K_d for the first class of K18Δ280-tau binding sites was 1.45 nM, indicating higher binding affinity to tau fibrils than to Aβ1–42 fibrils (K_d = 35.9 nM). Further, competitive binding assays with ^{18}F-THK-5105 displayed high binding affinity of phenylquinoline derivatives to tau fibrils (Fig. 3). The K_i for THK-5117 was 10.5 nM, indicating that THK-5117 has higher binding affinity for tau fibrils than THK-523 (K_i = 59.3 nM). In contrast, the K_i for FDDNP was 263 nM. In binding assays using mesial temporal brain homogenates containing a high density of tau (1,075 pmol/g) and moderate density of Aβ (434 pmol/g), both ^{18}F-THK-5105 (K_d = 2.63 nM; B_{max} = 358 pmol/g of tissue) and ^{18}F-THK-5117 (K_d = 5.19 nM; B_{max} = 338 pmol/g of tissue) showed higher affinity for mesial temporal brain homogenates than ^{18}F-THK-523 (K_d = 86.5 nM; B_{max} = 647.1 pmol/g of tissue) (Supplemental Fig. 1; supplemental materials are available online only at http://jnm.snmjournals.org).

Tissue Staining and Autoradiography

The selective binding ability of the compounds was further examined using AD brain sections. The fluorescent compound THK-5105 clearly stained NFTs and neuropil threads in the hippocampal section of an AD patient (Fig. 4A). Selective binding of this compound with tau pathology was confirmed by comparing with the results of tau immunohistochemistry for the same sections (Fig. 4B). In contrast, SPs were faintly stained with THK-5105. Further, we compared findings of THK-5105 staining with those of Gallyas–Braak silver staining, a conventional technique used to visualize tau pathology in the AD brain (Figs. 4C and 4D), and the binding of THK-5105 to NFTs and neuropil threads was confirmed. The images of staining with THK-5116 and THK-5117 were similar to those with THK-5105 (data not shown).

To investigate the binding ability of ^{18}F-THK-5105 and ^{18}F-THK-5117 to NFTs at tracer doses, in vitro autoradiography was performed in postmortem AD brain sections, and the findings were compared with Gallyas–Braak staining and immunohistochemistry. In the mesial temporal sections, laminar distributions of ^{18}F-THK-5105 and ^{18}F-THK-5117 were observed in the deep layer of gray matter (Fig. 5A). A high density of tracer accumulation was observed in the CA1 area of the hippocampus, which is reported as the most frequent site for NFTs in AD (*31*). These tracer distributions coincided with Gallyas–Braak staining and tau immunostaining (Fig. 5B) but not with the distribution of ^{11}C-PiB (Fig. 5A) and Aβ immunostaining (Fig. 5B). In contrast, no significant accumulation of ^{18}F-THK-5105 and ^{18}F-THK-5117 was observed in the hippocampus of the healthy control subject (Supplemental Fig. 2). ^{18}F-THK-5116 failed to give a specific signal in the AD brain sections (data not shown).

To further assess the regional differences of tracer binding in the AD brain, ^{18}F-THK-5105 autoradiography was conducted using AD hemibrain sections and compared with the Aβ PET tracer ^{11}C-PiB (*32*). ^{18}F-THK-5105 densely accumulated in the gray matter of the hippocampus, parahippocampal gyrus, fusiform gyrus, inferior and middle temporal gyri, insula, and cingulate gyrus (Fig. 6A), regions known for the abundance of tau pathology in AD (*33*). In contrast, tracer binding in the parietal areas was modest. The pattern of tracer distribution correlated with the known distribution of tau pathology (Fig. 6A) but not with the known distribution of Aβ or the binding of ^{11}C-PiB (data not shown). In addition, quantitative analyses of these images demonstrated a significant correlation of ^{18}F-THK-5105 binding with tau immunostained areas but not with the areas of Aβ immunostaining (Fig. 6B; Supplemental Fig. 3). In contrast, ^{11}C-PiB bindings showed a good correlation with Aβ deposition but not with tau deposition (Supplemental Fig. 3).

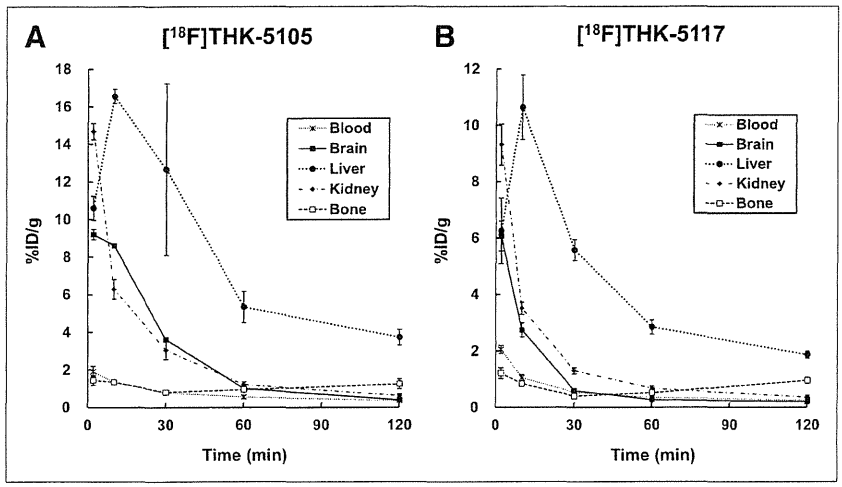

FIGURE 7. Time–activity curves after intravenous administration of ^{18}F-THK-5105 (A) and ^{18}F-THK-5117 (B) in mice.

Pharmacokinetics in Mice

All tested compounds exhibited sufficient amounts of tracer uptake in the mouse brain immediately after intravenous administration. Compared with ^{18}F-THK-523, new compounds showed significantly higher brain uptake at 2 min after injection (Table 1). ^{18}F-THK-5105 showed the highest brain uptake. In addition, clearance of these derivatives from normal brain tissue was faster than that of ^{18}F-THK-523 and ^{18}F-FDDNP (Table 1). The brain uptake ratio at 2 versus 60 min was highest for ^{18}F-THK-5117, followed by ^{18}F-THK-5105, ^{18}F-THK-5116, ^{18}F-FDDNP, and ^{18}F-THK-523. After injection of ^{18}F-THK-5105 and ^{18}F-THK-5117, the regional tracer uptake in the liver was highest at 10 min after injection, and the tracer was then slowly washed out from the body (Fig. 7). Compared with ^{18}F-THK-5105, ^{18}F-THK-5117 tended to have faster clearance from the brain, blood, liver, and kidney. No remarkable accumulation of ^{18}F-THK-5105 and ^{18}F-THK-5117 was observed in the bone.

Animal Toxicity Studies

A single intravenous administration of THK-5105 and THK-5117 at 1 mg/kg, equivalent to 100,000-fold the intended clinical dose for humans, caused no systemic toxicity in rats or mice. There were no unscheduled deaths or morbidity detected in this study. During the experimental period, the body weight of all animals increased normally, and no treatment-related changes were noted in any animals. There were no major clinical, biochemical, or histopathologic findings associated with the administration of THK-5105 and THK-5117.

Receptor Binding Assays

Binding inhibition of THK-5105 and THK-5117 was assessed in competitive radioligand binding assays against 60 common neurotransmitter receptors, ion channels, and transporters. As a result, no remarkable inhibition (<50%) was observed for various receptors, ion channels, and transporters at 1-μM concentrations of THK-5105 and THK-5117.

DISCUSSION

These findings suggest that ^{18}F-THK-5105 and ^{18}F-THK-5117 are promising candidates as tau imaging PET probes. Although previous saturation analysis showed the high binding affinity of ^{18}F-THK-523 for tau fibrils (K_d = 1.67 nM), the current competition assay demonstrated relatively lower binding affinity of THK-523 for tau fibrils (K_i = 59.3 nM) than THK-5105 (K_i = 7.8 nM) and THK-5117 (K_i = 10.5 nM). ^{18}F-THK-5105 showed higher affinity for tau pathology than for Aβ pathology in AD brain sections. Most amyloid imaging agents potentially bind to both tau and Aβ fibrils, because both protein fibrils share a common β-sheet secondary structure. To ensure the binding specificity of these compounds as tau-selective PET probes, the binding affinity to Aβ fibrils should be below the in vivo detection threshold. In vitro binding assays indicated that the binding affinity of ^{18}F-THK-5105 for Aβ fibrils (K_d = 35.9 nM) was 25 times lower than for tau fibrils (K_d = 1.45 nM). This K_d would allow selective detection of tau pathology, because the usual required K_d values for imaging Aβ are below 20 nM (*34*). However, the required K_d value for imaging tau deposits is still unknown. Considering that the concentrations of tau are about an order of magnitude lower than those of Aβ, the K_d value for tau should be well below 20 nM, in the low nanomolar range, to allow sensitive detection of tau pathology. In that respect, the binding affinities of both ^{18}F-THK-5105 and ^{18}F-THK-5117 to tau fibrils may be sufficient for in vivo detection of tau pathology in the brain. However, in vitro binding assay data should be carefully interpreted, because the structural conformation of synthetic tau fibrils does not fully correlate with the structure of NFTs and neuropil threads in the human brain. Actually, ^{18}F-THK-523 showed substantially lower affinity for AD brain homogenates (Kd = 86.5 nM) than for synthetic tau protein fibrils (Kd = 1.67 nM) (*15*). In the future, in vitro binding data should be compared with in vivo PET data to determine the required K_d value for in vivo tau detection.

In vitro assays using human brain samples are considered more reliable for evaluating the binding selectivity of radiotracers to tau and Aβ pathology at tracer doses. Autoradiography studies using human brain sections demonstrated the preferential binding of ^{18}F-THK-5105 and ^{18}F-THK-5117 to tau protein deposits in the AD brain. We observed a high density of ^{18}F-THK-5105 and ^{18}F-THK-5117 binding in the CA1 region of AD hippocampus, which contained substantial amounts of NFTs and neuropil threads. In addition, these tracers clearly visualized the laminar distribution of tau in the pri-α layer of the transentorhinal and temporal cortices, which is typically observed in the AD brain (*5*). The distribution pattern of THK tracer binding in AD brains was different from that of the Aβ imaging probe PiB and BF-227, which showed diffuse punctate distribution in broad neocortical gray matter and less tracer distribution in the mesial temporal region. These findings strongly suggest that binding properties of ^{18}F-THK-5105 and ^{18}F-THK-5117 are different from those of currently available Aβ PET probes. Compared with ^{18}F-THK-523 (*17*), both ^{18}F-THK-5105 and ^{18}F-THK-5117 showed higher contrast of tau pathology in autoradiographic images. These findings most likely reflect the increased binding affinity to tau by methylation of the amino group, as indicated by in vitro binding assays.

Similar findings were previously reported in an arylbenzothiazole derivative (*35*). Compared with ^{18}F-THK-5105, ^{18}F-THK-5117 showed lesser tracer binding in the gray matter containing high density of Aβ plaques, suggesting low binding affinity to Aβ and high selectivity to tau. ^{18}F-THK-5105 tends to show higher signals in the gray matter, and some of the images of ^{18}F-THK-5105 binding showed the patchy pattern as observed for ^{11}C-PiB binding. One possible reason for this is the binding of ^{18}F-THK-5105 to tau protein in dystrophic neurites. Another possible reason is binding of ^{18}F-THK-5105 to Aβ fibrils. However, the latter explanation seems unlikely given that ^{18}F-THK-5105 binding, as clearly shown in Figure 6, was correlated with tau, and not Aβ, deposits.

In vitro binding assays using AD brain homogenates are generally used to measure the binding affinity of Aβ imaging radiotracers to SPs or NFTs and the number of binding sites in real AD pathology (*36*). For most of the useful Aβ imaging radiotracers, the reported K_d or K_i values for neocortical brain samples are below 10 nM (*36,37*). In this study, the K_d values for high-affinity sites of AD mesial temporal homogenates were 2.63 nM for ^{18}F-THK-5105 and 5.19 nM for ^{18}F-THK-5117. These binding affinities were higher than that for ^{18}F-THK-523 and appear to be sufficient for the in vivo detection of AD pathology in the mesial temporal region at tracer doses. Furthermore, the B_{max}/K_d ratios of ^{18}F-THK-5105 and ^{18}F-THK-5117 for AD brain homogenates were 136.1 and 65.1, respectively, which fulfills the criteria (B_{max}/K_d ratio > 10) for a good neuroimaging agent (*35*).

The optimization of pharmacokinetics is an important aspect in the development of a PET tracer (*38*). ^{18}F-THK-5105, ^{18}F-THK-5116, and ^{18}F-THK-5117 fulfilled the criteria of appropriate log P value (log P = 1–3) for brain entry (*39*). In mice, these tracers showed sufficient brain uptake and rapid washout from normal brain tissue. ^{18}F-THK-5105 and ^{18}F-THK-5117 exhibited high initial brain uptake in normal mice (>6 %ID/g at 2 min). These values, which are equivalent to over 100% injected dose index in a 25-g mouse, meet the prerequisites for useful PET imaging agents (*34*). The 2- to 60-min ratio of radioactivity concentrations for ^{18}F-THK-5117 was 23.1, indicating faster washout from normal brain for these compounds than for other currently available ^{18}F-labeled tracers such as ^{18}F-FDDNP (2.91), ^{18}F-florbetaben (4.83) (*40*), and ^{18}F-florbetapir (3.90) (*37*). Compared with ^{18}F-THK-523, ^{18}F-THK-5116 washed out faster from normal brain tissue of mice, indicating that the hydroxylation of the fluoroalkoxy group improves pharmacokinetics in mice. However ^{18}F-THK-5116 is not a suitable compound for clinical application, because of its lower initial brain uptake and binding affinity than the other 2 compounds.

CONCLUSION

^{18}F-THK-5105 and ^{18}F-THK-5117 should be considered as promising candidates for PET tau imaging radiotracers. Future clinical studies will clarify the usefulness of these radiotracers for the early detection of AD tau pathology.

DISCLOSURE

The costs of publication of this article were defrayed in part by the payment of page charges. Therefore, and solely to indicate this fact, this article is hereby marked "advertisement" in accordance with 18 USC section 1734. This study was supported by the research fund from GE Healthcare; the Industrial Technology Research Grant Program of the NEDO in Japan (09E51025a); Health and Labor Sciences Research grants from the Ministry of Health, Labor, and Welfare of Japan; and a Grant-in-Aid for Scientific Research (B) (23390297) and "Japan Advanced Molecular Imaging Program (J-AMP)" of the Ministry of Education, Culture, Sports, Science and Technology (MEXT), Japan. No other potential conflict of interest relevant to this article was reported.

REFERENCES

1. Organisation for Economic Co-operation and Development (OECD). *Understanding the Brain: The Birth of a Learning Science*. Paris, France: OECD Publishing, 2007.
2. Hardy J, Selkoe DJ. The amyloid hypothesis of Alzheimer's disease: progress and problems on the road to therapeutics. *Science*. 2002;297:353–356.
3. Lichtenberg B, Mandelkow EM, Hagestedt T, Mandelkow E. Structure and elasticity of microtubule-associated protein tau. *Nature*. 1988;334:359–362.
4. Holzer M, Holzapfel HP, Zedlick D, Bruckner MK, Arendt T. Abnormally phosphorylated tau protein in Alzheimer's disease: heterogeneity of individual regional distribution and relationship to clinical severity. *Neuroscience*. 1994;63:499–516.
5. Braak H, Braak E. Neuropathological stageing of Alzheimer-related changes. *Acta Neuropathol*. 1991;82:239–259.
6. Bondareff W, Mountjoy CQ, Roth M, Hauser DL. Neurofibrillary degeneration and neuronal loss in Alzheimer's disease. *Neurobiol Aging*. 1989;10:709–715.
7. Bobinski M, Wegiel J, Wisniewski HM, et al. Neurofibrillary pathology: correlation with hippocampal formation atrophy in Alzheimer disease. *Neurobiol Aging*. 1996;17:909–919.
8. Guillozet AL, Weintraub S, Mash DC, Mesulam MM. Neurofibrillary tangles, amyloid, and memory in aging and mild cognitive impairment. *Arch Neurol*. 2003;60:729–736.
9. Gómez-Isla T, Price JL, McKeel DW Jr., Morris JC, Growdon JH, Hyman BT. Profound loss of layer II entorhinal cortex neurons occurs in very mild Alzheimer's disease. *J Neurosci*. 1996;16:4491–4500.
10. Okamura N, Suemoto T, Furumoto S, et al. Quinoline and benzimidazole derivatives: candidate probes for in vivo imaging of tau pathology in Alzheimer's disease. *J Neurosci*. 2005;25:10857–10862.
11. Rojo LE, Alzate-Morales J, Saavedra IN, Davies P, Maccioni RB. Selective interaction of lansoprazole and astemizole with tau polymers: potential new clinical use in diagnosis of Alzheimer's disease. *J Alzheimers Dis*. 2010;19:573–589.
12. Ono M, Hayashi S, Matsumura K, et al. Rhodanine and thiohydantoin derivatives for detecting tau pathology in Alzheimer's brains. *ACS Chem Neurosci*. 2011;2:269–275.
13. Jensen JR, Cisek K, Funk KE, Naphade S, Schafer KN, Kuret J. Research towards tau imaging. *J Alzheimers Dis*. 2011;26(suppl 3):147–157.
14. Zhang W, Arteaga J, Cashion DK, et al. A highly selective and specific PET tracer for imaging of tau pathologies. *J Alzheimers Dis*. 2012;31:601–612.
15. Fodero-Tavoletti MT, Okamura N, Furumoto S, et al. ^{18}F-THK523: a novel in vivo tau imaging ligand for Alzheimer's disease. *Brain*. 2011;134:1089–1100.
16. Villemagne VL, Furumoto S, Fodero-Tavoletti MT, et al. The challenges of tau imaging. *Future Neurol*. 2012;7:409–421.
17. Harada R, Okamura N, Furumoto S, et al. Comparison of the binding characteristics of [^{18}F]THK-523 and other amyloid imaging tracers to Alzheimer's disease pathology. *Eur J Nucl Med Mol Imaging*. 2013;40:125–132.
18. Small GW, Agdeppa ED, Kepe V, Satyamurthy N, Huang SC, Barrio JR. In vivo brain imaging of tangle burden in humans. *J Mol Neurosci*. 2002;19:323–327.
19. Agdeppa ED, Kepe V, Liu J, et al. Binding characteristics of radiofluorinated 6-dialkylamino-2-naphthylethylidene derivatives as positron emission tomography imaging probes for beta-amyloid plaques in Alzheimer's disease. *J Neurosci*. 2001;21:RC189.
20. Thompson PW, Ye L, Morgenstern JL, et al. Interaction of the amyloid imaging tracer FDDNP with hallmark Alzheimer's disease pathologies. *J Neurochem*. 2009;109:623–630.
21. Tolboom N, Yaqub M, van der Flier WM, et al. Detection of Alzheimer pathology in vivo using both ^{11}C-PIB and ^{18}F-FDDNP PET. *J Nucl Med*. 2009;50:191–197.
22. Shoghi-Jadid K, Small GW, Agdeppa ED, et al. Localization of neurofibrillary tangles and beta-amyloid plaques in the brains of living patients with Alzheimer disease. *Am J Geriatr Psychiatry*. 2002;10:24–35.

23. Näslund J, Haroutunian V, Mohs R, et al. Correlation between elevated levels of amyloid beta-peptide in the brain and cognitive decline. *JAMA.* 2000;283: 1571–1577.
24. Mukaetova-Ladinska EB, Harrington CR, Roth M, Wischik CM. Biochemical and anatomical redistribution of tau protein in Alzheimer's disease. *Am J Pathol.* 1993;143:565–578.
25. Liu J, Kepe V, Zabjek A, et al. High-yield, automated radiosynthesis of 2-(1-{6-[(2-[^{18}F]fluoroethyl)(methyl)amino]-2-naphthyl}ethylidene)malononitrile ([^{18}F] FDDNP) ready for animal or human administration. *Mol Imaging Biol.* 2007;9:6–16.
26. Fodero-Tavoletti MT, Mulligan RS, Okamura N, et al. In vitro characterisation of BF227 binding to alpha-synuclein/Lewy bodies. *Eur J Pharmacol.* 2009;617:54–58.
27. Wilson AA, Garcia A, Chestakova A, Kung H, Houle S. A rapid one-step radiosynthesis of the beta-amyloid imaging radiotracer N-methyl-[C-11]2-(4′-methylaminophenyl)-6-hydroxybenzothiazole ([C-11]-6-OH-BTA-1). *J Labelled Comp Radiopharm.* 2004;47:679–682.
28. Cheng Y, Prusoff WH. Relationship between the inhibition constant (Ki) and the concentration of inhibitor which causes 50 per cent inhibition (IC50) of an enzymatic reaction. *Biochem Pharmacol.* 1973;22:3099–3108.
29. Okamura N, Suemoto T, Shimadzu H, et al. Styrylbenzoxazole derivatives for in vivo imaging of amyloid plaques in the brain. *J Neurosci.* 2004;24: 2535–2541.
30. Ikeda K, Akiyama H, Kondo H, Haga C. A study of dementia with argyrophilic grains. Possible cytoskeletal abnormality in dendrospinal portion of neurons and oligodendroglia. *Acta Neuropathol.* 1995;89:409–414.
31. Bouras C, Hof PR, Giannakopoulos P, Michel JP, Morrison JH. Regional distribution of neurofibrillary tangles and senile plaques in the cerebral cortex of elderly patients: a quantitative evaluation of a one-year autopsy population from a geriatric hospital. *Cereb Cortex.* 1994;4:138–150.
32. Kudo Y, Okamura N, Furumoto S, et al. 2-(2-[2-Dimethylaminothiazol-5-yl] ethenyl)-6- (2-[fluoro]ethoxy)benzoxazole: a novel PET agent for in vivo detection of dense amyloid plaques in Alzheimer's disease patients. *J Nucl Med.* 2007;48:553–561.
33. Braak H, Alafuzoff I, Arzberger T, Kretzschmar H, Del Tredici K. Staging of Alzheimer disease-associated neurofibrillary pathology using paraffin sections and immunocytochemistry. *Acta Neuropathol.* 2006;112:389–404.
34. Mathis CA, Wang Y, Klunk WE. Imaging beta-amyloid plaques and neurofibrillary tangles in the aging human brain. *Curr Pharm Des.* 2004;10:1469–1492.
35. Mathis CA, Wang Y, Holt DP, Huang GF, Debnath ML, Klunk WE. Synthesis and evaluation of ^{11}C-labeled 6-substituted 2-arylbenzothiazoles as amyloid imaging agents. *J Med Chem.* 2003;46:2740–2754.
36. Klunk WE, Wang Y, Huang GF, et al. The binding of 2-(4′-methylaminophenyl) benzothiazole to postmortem brain homogenates is dominated by the amyloid component. *J Neurosci.* 2003;23:2086–2092.
37. Choi SR, Golding G, Zhuang Z, et al. Preclinical properties of ^{18}F-AV-45: a PET agent for Abeta plaques in the brain. *J Nucl Med.* 2009;50:1887–1894.
38. Furumoto S, Okamura N, Iwata R, Yanai K, Arai H, Kudo Y. Recent advances in the development of amyloid imaging agents. *Curr Top Med Chem.* 2007;7:1773–1789.
39. Waterhouse RN. Determination of lipophilicity and its use as a predictor of blood-brain barrier penetration of molecular imaging agents. *Mol Imaging Biol.* 2003;5:376–389.
40. Zhang W, Oya S, Kung MP, Hou C, Maier DL, Kung HF. F-18 Polyethyleneglycol stilbenes as PET imaging agents targeting Abeta aggregates in the brain. *Nucl Med Biol.* 2005;32:799–809.

Neuron
Article

Imaging of Tau Pathology in a Tauopathy Mouse Model and in Alzheimer Patients Compared to Normal Controls

Masahiro Maruyama,[1,10] Hitoshi Shimada,[1,10] Tetsuya Suhara,[1] Hitoshi Shinotoh,[1] Bin Ji,[1] Jun Maeda,[1] Ming-Rong Zhang,[1] John Q. Trojanowski,[2] Virginia M.-Y. Lee,[2] Maiko Ono,[1] Kazuto Masamoto,[1] Harumasa Takano,[1] Naruhiko Sahara,[3,5,6] Nobuhisa Iwata,[4] Nobuyuki Okamura,[7] Shozo Furumoto,[7] Yukitsuka Kudo,[8] Qing Chang,[9] Takaomi C. Saido,[4] Akihiko Takashima,[3] Jada Lewis,[5,6] Ming-Kuei Jang,[9] Ichio Aoki,[1] Hiroshi Ito,[1] and Makoto Higuchi[1,*]
[1]Molecular Imaging Center, National Institute of Radiological Sciences, 4-9-1 Anagawa, Inage-ku, Chiba, Chiba 263-8555, Japan
[2]Center for Neurodegenerative Disease Research, University of Pennsylvania Perelman School of Medicine, Third Floor HUP-Maloney, 36th and Spruce Streets, Philadelphia, PA 19104, USA
[3]Laboratory for Alzheimer's Disease
[4]Laboratory for Proteolytic Neuroscience
RIKEN Brain Science Institute, 2-1 Hirosawa, Wako, Saitama 351-0198, Japan
[5]Center for Translational Research in Neurodegenerative Disease
[6]Department of Neuroscience
University of Florida, 1275 Center Drive, Gainesville, FL 32610, USA
[7]Department of Pharmacology, Tohoku University Graduate School of Medicine, 2-1 Seiryo-machi, Aoba-ku, Sendai, Miyagi 980-8575, Japan
[8]Clinical Research, Innovation and Education Center, Tohoku University Hospital, 1-1 Seiryo-machi, Aoba-ku, Sendai, Miyagi 980-8574, Japan
[9]Institute for Applied Cancer Science, MD Anderson Cancer Center, 1901 East Road, Houston, TX 77054, USA
[10]These authors contributed equally to this work
*Correspondence: mhiguchi@nirs.go.jp
http://dx.doi.org/10.1016/j.neuron.2013.07.037

SUMMARY

Accumulation of intracellular tau fibrils has been the focus of research on the mechanisms of neurodegeneration in Alzheimer's disease (AD) and related tauopathies. Here, we have developed a class of tau ligands, phenyl/pyridinyl-butadienyl-benzothiazoles/benzothiazoliums (PBBs), for visualizing diverse tau inclusions in brains of living patients with AD or non-AD tauopathies and animal models of these disorders. In vivo optical and positron emission tomographic (PET) imaging of a transgenic mouse model demonstrated sensitive detection of tau inclusions by PBBs. A pyridinated PBB, [^{11}C]PBB3, was next applied in a clinical PET study, and its robust signal in the AD hippocampus wherein tau pathology is enriched contrasted strikingly with that of a senile plaque radioligand, [^{11}C]Pittsburgh Compound-B ([^{11}C]PIB). [^{11}C]PBB3-PET data were also consistent with the spreading of tau pathology with AD progression. Furthermore, increased [^{11}C]PBB3 signals were found in a corticobasal syndrome patient negative for [^{11}C]PIB-PET.

INTRODUCTION

Hallmark pathologies of Alzheimer's disease (AD) are extracellular senile plaques consisting of aggregated amyloid β peptide (Aβ) and intraneuronal neurofibrillary tangles (NFTs) composed of pathological tau fibrils, while similar tau lesions in neurons and glia are also characteristic of other neurodegenerative disorders, such as progressive supranuclear palsy (PSP) and corticobasal degeneration (CBD), that are collectively referred to as tauopathies (Ballatore et al., 2007). The discovery of *tau* gene mutations in a familial form of tauopathy, known as frontotemporal dementia and parkinsonism linked to chromosome 17 (FTDP-17), and subsequent studies of transgenic (Tg) mice expressing human tau with or without these mutations, clearly implicate pathological tau in mechanisms of neurodegeneration in AD and related tauopathies (Ballatore et al., 2007). Thus, there is an urgent need for tau imaging techniques to complement Aβ amyloid imaging methods that now are widely used.

In vivo imaging modalities, as exemplified by positron emission tomography (PET) (Klunk et al., 2004; Small et al., 2006; Kudo et al., 2007; Maeda et al., 2007), optical scanning (Bacskai et al., 2003; Hintersteiner et al., 2005), and magnetic resonance imaging (MRI) (Higuchi et al., 2005), have enabled visualization of Aβ deposits in humans with AD and/or AD mouse models, and there has been a growing expectation that low-molecular-weight ligands for β-pleated sheet structures will also serve as molecular probes for tau amyloids. Although the majority of plaque-imaging agents used for clinical PET studies do not bind to tau lesions (Klunk et al., 2003), at least one radiolabeled β sheet ligand, [^{18}F]FDDNP, enables PET imaging of AD NFTs (Small et al., 2006). However, a relatively low contrast of in vitro autoradiographic and in vivo PET signals for [^{18}F]FDDNP putatively reflecting tau lesions does not allow a simple visual inspection of images for the assessment of tau pathologies in living subjects